Chemical Science

ROYAL SOCIETY OF CHEMISTRY

EDGE ARTICLE

View Article Online
View Journal

Cite this: DOI: 10.1039/d5sc02914g

All publication charges for this article have been paid for by the Royal Society of Chemistry

Received 21st April 2025
Accepted 22nd August 2025

DOI: 10.1039/d5sc02914g

rsc.li/chemical-science

Geminal hyperconjugation as a driving force for C–C bond shortening in heavy-atom tunnelling

Croix J. Laconsay,[a] Ishika Jain,[b] Tim Schleif,*[c] William L. Karney*[b] and Judy I. Wu*[a]

Quantum mechanical tunnelling significantly influences the reactivity of strained ring systems, yet strategies for controlling such reactivity remain largely unexplored. Here, we identify geminal hyperconjugation, *i.e.*, electron delocalization between σ-bonds attached to a common atom, as a decisive electronic factor in governing heavy-atom tunnelling reactions involving three-membered rings. We illustrate this through a case study of the oxepin (**1′**) ⇌ benzene oxide (**1**) equilibrium, recently shown to undergo solvent-controlled tunnelling at 3 K (*Angew. Chem. Int. Ed.*, 2020, **59**, 20318). Natural bond orbital analyses reveal that coordination of ICF_3, H_2O, or H^+ to the oxygen atom of **1** enhances geminal C–O σ → O–C σ* delocalization in the oxirane ring, strengthening the C(1)–C(6) bond, and facilitating the **1′** to **1** rearrangement. Tunnelling-inclusive Arrhenius plots show increasingly large deviations from a linear relationship for the electrocyclizations of **1′** → **1**, **1′**-$2H_2O$ → **1**-$2H_2O$, and **1′**-H^+ → **1**-H^+. Related cases, including benzene sulfide (**1S**), oxirane (**2**), and benzazirine (**3**), are examined.

Introduction

Heavy-atom tunnelling in organic molecules is often associated with strained ring systems, such as benzene oxide, benzene imine, norcaradiene, semibullvalene, and benzazirine, and often involves opening and closing three-membered rings.[1–11] While ring strain is typically attributed to geometric distortion and angle compression, subtle electronic effects may also influence such transformations. One such effect is geminal hyperconjugation, *i.e.*, a donor–acceptor interaction between neighbouring σ-bonds attached to a common atom. Although rarely emphasized in conventional chemical explanations, geminal hyperconjugation becomes particularly relevant in molecules with acute bond angles, such as those containing three-membered ring motifs. Geminal electron delocalization effects can contribute to reducing strain energy and modulating chemical reactivity.[12,13] Fig. 1a shows a schematic illustration of geminal hyperconjugation and its accompanying geometric consequences. Back and forth A–B σ → A–C σ* and A–C σ → A–B σ* delocalizations elongate the A–B and A–C bonds and simultaneously shorten the B–C bond. Considering these geometric changes, we wondered if geminal hyperconjugations leading to shortened B–C bonds in three-membered ring motifs could facilitate heavy-atom tunnelling reactions.

A compelling example of heavy-atom tunnelling modulated by environmental factors is the equilibrium between benzene oxide (**1**) and its valence tautomer oxepin (**1′**) (Fig. 1b). In 2020, Schleif, Prado Merini, and Sander reported that this equilibrium, which proceeds *via* ring-opening and ring-closing of a three-membered ring epoxide unit, is highly sensitive to solvent interactions.[14] At 3 K in solid argon, **1** undergoes ring-opening to form **1′**. However, when **1′** is complexed by a single molecule of H_2O or ICF_3, the direction of tunnelling reverses, and complexed **1′** undergoes ring-closure to form complexed **1**. This solvent-controlled reversal of tunnelling direction is intriguing, as it suggests that even subtle changes in local electronic environments can significantly alter the thermodynamic driving force and influence the reaction barrier width. More broadly, the **1** ⇌ **1′** equilibrium may be viewed as a special case of tunnelling catalysis[15] of epoxide ring-opening, where coordination by even a single solvent molecule influences the efficiency of bond rearrangements.

The structural rearrangement between **1** ⇌ **1′** involves a disrotatory electrocyclic reaction with minimal motion of the C(1)

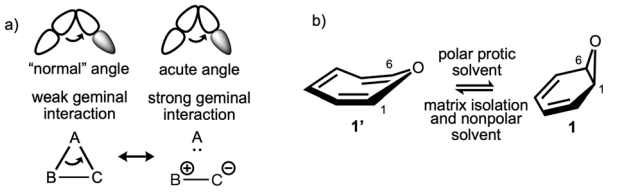

Fig. 1 (a) Schematic illustration of geminal hyperconjugation. (b) Equilibrium between oxepin (**1′**) and benzene oxide (**1**).

[a]Department of Chemistry, University of Houston, Houston, Texas 77204, USA. E-mail: jiwu@central.uh.edu

[b]Department of Chemistry, University of San Francisco, San Francisco, California 94117, USA. E-mail: karney@usfca.edu

[c]Department of Chemistry, Hofstra University, Hempstead, NY 11549-1000, USA. E-mail: tim.schleif@hofstra.edu

and C(6) atoms, making it a prototypical system for studying tunnelling through narrow barriers. Interestingly, solvent effects on the equilibrium of this tautomeric pair had already been noted in earlier works. Vogel, Böll, and Günther[16] observed that the equilibrium favors oxepin (**1′**) in nonpolar solvents such as isooctane, but shifts towards benzene oxide (**1**) in polar protic mixtures like in water–methanol solutions. Stohrer and Hoffmann offered a qualitative explanation, proposing that protonation or coordination of the heteroatom lone pair strengthens adjacent C–C bonds in oxiranes and aziridines.[17] Yet, a mechanistic rationale for the solvent dependence of the tunnelling equilibrium remains lacking. In this work, we explore the hypothesis that enhanced geminal hyperconjugation and solvent-induced bond changes can significantly alter the thermodynamic driving force and the barrier widths relevant to heavy-atom tunnelling.

Results and discussion

We begin by comparing the computed natural bond orbital (NBO)[18,19] second-order perturbation energies $E(2)$ for propane, cyclopropane, oxirane (**2**), and protonated oxirane (**2**-H^+) to establish that: (1) acute bond angles are necessary for large geminal hypeconjugative effects to occur, and that, (2) geminal electron delocalizations are tunable by coordination. As shown in Fig. 2a, the geminal C–C σ → C–C σ* interactions in propane (0.3 kcal mol^{-1} per interaction) are negligible and contrast with the much larger values for cyclopropane (5.1 kcal mol^{-1} per interaction). Geminal orbital interactions were first put forth by Weinhold and Landis,[12] and by Inagaki,[20,21] and later, by Wu and Schleyer,[22] to explain the unusually low ring strain of cyclopropane. Like cyclopropane, oxirane (**2**) exhibits a large geminal C–O σ → O–C σ* stabilization (5.9 kcal mol^{-1} per interaction at the O vertex). Note that **2** also exhibits C–C σ → O–C σ* and O–C σ → C–C σ* geminal interactions at the C vertices, but the corresponding $E(2)$ values are small (<3 kcal mol^{-1}) (see data in the SI). Remarkably, upon coordination of a proton to the oxygen atom, **2**-H^+ displays significantly increased C–O σ → O–C σ* interaction (8.9 kcal mol^{-1} per interaction), which can be explained by the donor and acceptor abilities of the C–O σ and O–C σ* orbitals. Protonation at the oxygen atom makes O–C σ* a much better acceptor and increases C–O σ → O–C σ* delocalization. As a result, the C–O bonds weaken and the C–C bond strengthens. These geometric changes further explain the acid-catalyzed ring-opening of epoxides.[23]

We now show that the same electronic effect influences the equilibrium of **1′** ⇌ **1** upon coordination of the oxygen atom in benzene oxide (**1**) to two molecules of ICF_3, two molecules of H_2O, or H^+. We also examined related ring systems containing three-membered ring motifs, such as benzene sulfide (**1S**), oxirane (**2**), and benzazirine (**3**). Second-order perturbation energies $E(2)$ for the uncomplexed and complexed derivatives are compared in Table 1 (see structures in Fig. 2).

As shown in Table 1, coordination of a Lewis acid to the oxygen lone pair of **1** increases geminal C–O σ → O–C σ* interaction in the order: **1** (5.8 kcal mol^{-1}) < **1**-2ICF_3 (6.6 kcal mol^{-1}) ≈ **1**-2H_2O (6.6 kcal mol^{-1}) < **1**-H^+ (10.0 kcal mol^{-1}). Accordingly, the ∠COC bond angles become narrower: **1** (64.2°), **1**-2ICF_3 (63.3°), **1**-2H_2O (63.1°), **1**-H^+ (56.8°), and the C(1)–C(6) bonds shorten: **1** (1.506 Å) > **1**-2ICF_3 (1.499 Å) = **1**-2H_2O (1.499 Å) > **1**-H^+ (1.475 Å). In agreement, NBO calculations show decreased p character for the C(1)–C(6) bonds in the order: **1** ($sp^{4.00}$, *i.e.*, weaker C(1)–C(6) bond) > **1**-2ICF_3 ($sp^{3.83}$) ≈ **1**-2H_2O ($sp^{3.84}$) > **1**-H^+ ($sp^{2.96}$, *i.e.*, stronger C(1)–C(6) bond) (see Table 1). These results show that coordination of the oxygen atom in benzene oxide (**1**) strengthens the C(1)–C(6) bond as a result of enhanced geminal C–O σ → O–C σ* interaction.

Also notable is the increasingly large thermodynamic driving force favoring **1** as evidenced by the computed energies (ΔE_{rel})

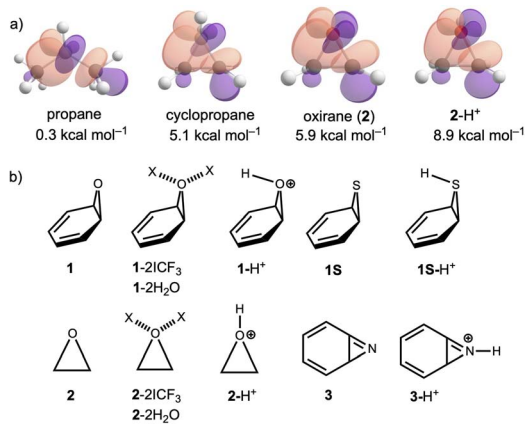

Fig. 2 (a) Computed NBO $E(2)$ energies for propane (C–C σ → C–C σ*), cyclopropane (C–C σ → C–C σ*), oxirane (C–O σ → O–C σ*), and protonated oxirane (C–O σ → O–C σ*). (b) Uncomplexed and complexed benzene oxide (**1**), benzene sulfide (**1S**), oxirane (**2**), and benzazirine (**3**) species investigated.

Table 1 Computed $E(2)$ C–X σ → X–C σ* interaction energies (in kcal mol^{-1}), C–C[a] and C–X bonds (in Å), and bond hybridizations for benzene oxide (**1**), benzene sulfide (**1S**), oxirane (**2**), and benzazirine (**3**) and their coordinated analogues

Cmpd	$E(2)$	∠CXC	C(1)–C(6)[a]	C–X	C(1)–C(6)[a] hybridization
1	5.8	64.2	1.506	1.417	$sp^{4.00}$
1-2ICF_3	6.6	63.3	1.499	1.430	$sp^{3.83}$
1-2H_2O	6.6	63.1	1.499	1.432	$sp^{3.84}$
1-H^+	10.0	56.8	1.475	1.552	$sp^{2.96}$
1S	7.9	47.8	1.489	1.836	$sp^{2.86}$
1S-H^+	14.4	44.3	1.463	1.942	$sp^{2.48}$
2	5.9	61.9	1.456	1.415	$sp^{3.36}$
2-2ICF_3	6.8	61.4	1.455	1.425	$sp^{3.11}$
2-2H_2O	6.9	61.0	1.454	1.432	$sp^{3.11}$
2-H^+	8.9	57.7	1.452	1.505	$sp^{2.74}$
3	2.2[b]	63.1	1.480	1.246[d]	$sp^{3.73}$
	4.1[c]			1.542[e]	
3-H^+	1.0[b]	62.0	1.463	1.275[d]	$sp^{3.14}$
	7.2[c]			1.534[e]	

[a] C–C bond in three-membered ring. [b] C=N σ → N–C σ*. [c] N–C σ → C=N σ*. [d] C=N bond in azirine ring. [e] N–C bond in azirine ring.

for **1** (+1.0 kcal mol^{-1}), **1**-2ICF$_3$ (−0.3 kcal mol^{-1}), **1**-2H$_2$O (−0.7 kcal mol^{-1}), and **1**-H$^+$ (−9.8 kcal mol^{-1}) relative to their respective oxepin isomers at DLPNO-CCSD(T)/def2-TZVP//PW6B95/def2-TZVP (Fig. 3). By assuming a linear relationship between carbon–carbon bond lengths and bond dissociation energies,[24] the difference in equilibrium bond lengths for **1** (1.506 Å) *vs.* **1**-H$^+$ (1.475 Å) can correspond to an increase of 10–15 kcal mol^{-1} in the C(sp^3)–C(sp^3) bond dissociation energy, which matches the ≈11 kcal mol^{-1} greater driving force for **1′**-H$^+$ → **1**-H$^+$.

We further examined the computed $E(2)$ C–O σ → O–C σ* energies for the electrocyclic ring-opening transition structures of **1**-TS (3.3 kcal mol^{-1}), **1**-2ICF$_3$-TS (3.4 kcal mol^{-1}), **1**-2H$_2$O-TS (3.4 kcal mol^{-1}), and **1**-H$^+$-TS (3.4 kcal mol^{-1}) and found them to be nearly unchanged across the series (Fig. 3). This suggests that Lewis acid coordination affects the driving force for ring-closure, but does not affect the kinetic barriers. Indeed, computed activation barriers ($\Delta E^{\ddagger}$) for **1′** → **1** (8.4 kcal mol^{-1}), **1′**-2ICF$_3$ → **1**-2ICF$_3$ (8.0 kcal mol^{-1}), **1′**-2H$_2$O → **1**-2H$_2$O (7.7 kcal mol^{-1}), and **1′**-H$^+$ → **1**-H$^+$ (8.7 kcal mol^{-1}) at the DLPNO-CCSD(T)/def2-TZVP//PW6B95/def2-TZVP level are nearly the same (Fig. 3). Note that **1**-H$^+$-TS displays the longest C(1)···C(6) distance, which indicates an early transition state and aligns with a strongly exothermic reaction.

We also examined the effects of geminal hyperconjugation in benzene sulfide (**1S**) (the sulfur analog of benzene oxide) and observed an even greater enhancement of geminal C–S σ → S–C σ* hyperconjugation upon protonation to form **1S**-H$^+$. As shown in Table 1, the computed $E(2)$ C–S σ → S–C σ* interaction increases from 7.9 kcal mol^{-1} in **1S** to 14.4 kcal mol^{-1} in protonated **1S**-H$^+$. This increase in geminal hyperconjugation correlates to a narrowing of the ∠CSC bond angle (47.8° in **1S** *vs.* 44.3° in **1S**-H$^+$) and shortening of the C(1)–C(6) bond (1.489 Å *vs.* 1.463 Å). The C(1)–C(6) bond in **1S**-H$^+$ also exhibits decreased p character, as reflected by the change in hybridization from **1S** (sp$^{2.86}$) to **1S**-H$^+$ (sp$^{2.48}$). These results suggest that geminal hyperconjugation plays an even more pronounced role in benzene sulfide than in benzene oxide, and predict that solvent or Lewis acid coordination could strongly promote ring-closure *via* heavy-atom tunnelling in this system.

Similar trends were observed for oxirane (**2**). Lewis acid coordination at the oxygen atom increases geminal C–O σ → O–C σ* interaction in the order: **2** (5.9 kcal mol^{-1}) < **2**-2ICF$_3$ (6.8 kcal mol^{-1}) ≈ **2**-2H$_2$O (6.9 kcal mol^{-1}) < **2**-H$^+$ (8.9 kcal mol^{-1}). The ∠COC bond angles become narrower: **2** (61.9°) > **2**-2ICF$_3$ (61.4°) > **2**-2H$_2$O (61.0°) > **2**-H$^+$ (57.7°), and the C–C bonds shorten: **2** (1.456 Å) < **2**-2ICF$_3$ (1.455 Å) < **2**-2H$_2$O (1.454 Å) < **2**-H$^+$ (1.452 Å). Although the C–C bonds shorten only slightly upon Lewis acid coordination, the computed hybridizations of the C–C bonds show a notable decrease in p character: **2** (sp$^{3.36}$, weaker C–C bond) > **2**-2ICF$_3$ (sp$^{3.11}$) ≈ **2**-2H$_2$O (sp$^{3.11}$) > **2**-H$^+$ (sp$^{2.74}$, stronger C–C bond). Thus, the acid-catalyzed ring-opening of epoxides may be viewed as a consequence of enhanced geminal hyperconjugation due to protonation at the oxygen atom.[23]

Benzazirine (**3**), like benzene oxide, contains an annelated six- and three-membered ring. Compound **3** can undergo ring-opening of the azirine motif through quantum mechanical tunnelling.[4–11] Depending on the substitution pattern, tunnelling of either the nitrogen atom (C–N bond breaking) or a carbon atom (C–C bond breaking) leads to formation of an aryl nitrene or a seven-membered ring cyclic ketenimine, respectively.[4,5] Second-order perturbation energies $E(2)$ computed for **3** reveal a weak C=N σ → N–C σ* interaction (2.2 kcal mol^{-1}) and a modest N–C σ → C=N σ* interaction (4.1 kcal mol^{-1}). Upon protonation to give **3**-H$^+$, the C=N σ → N–C σ* interaction remains nearly unchanged (1.0 kcal mol^{-1}), whereas the N–C σ → C=N σ* interaction increases notably (7.2 kcal mol^{-1}). This suggests that protonation at the nitrogen atom enhances the electron accepting ability of the C=N σ* orbital. Protonation also shortens the C(1)–C(6) bond (1.480 Å for **3** and 1.463 Å for **3**-H$^+$) and reduces its p character (from sp$^{3.73}$ to sp$^{3.14}$). These changes predict that protonation at the nitrogen atom should favor tunnelling pathways leading to aryl nitrenium formation.

Next, we show that a strong thermodynamic driving force is connected to a narrower reaction barrier width. Quantum mechanical tunnelling is a direct result of the wave-like nature of atoms. Unlike over-the-barrier reactions, in which the barrier height solely determines the rate of reaction, the probability of tunnelling (P) is impacted by atomic mass (m), activation energy (E_A) and the barrier width (w) (eqn (1)).[25–28]

$$P \approx e^{-w\pi^2\sqrt{2mE_A}/h} \quad (1)$$

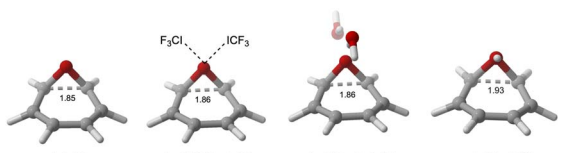

	1-TS	**1**-2ICF$_3$-TS	**1**-2H$_2$O-TS	**1**-H$^+$-TS
ΔE_{rel}	+1.0	−0.3	−0.7	−9.8
$\Delta E^{\ddagger}$	8.4	8.0	7.7	8.7
C(1)…C(6)	1.847	1.860	1.861	1.929

Fig. 3 Transition state structures, activation barriers (in kcal mol^{-1}) for the electrocyclizations of uncomplexed and complexed **1′** → **1**, and C(1)···C(6) distances (in Å) for **1**-TS, **1**-2ICF$_3$-TS, **1**-2H$_2$O-TS, and **1**-H$^+$-TS at DLPNO-CCSD(T)/def2-TZVP//PW6B95/def2-TZVP.

The intrinsic barrier width of a reaction reflects the reorganization energy required for the nuclear coordinates of the reactant to become those of the product at zero driving force (*i.e.*, $\Delta G = 0$). In an authoritative perspective, Qiu and Schreiner pointed out that when the driving force for tunnelling is non-zero, a larger free energy change between the reactant and product can give rise to a narrower barrier width.[29] Indeed, computed vibrationally adiabatic ground-state potential energy (V_a^G) curves for the interconversion of **1′** ⇌ **1**, **1′**-2ICF$_3$ ⇌ **1**-2ICF$_3$, **1′**-2H$_2$O ⇌ **1**-2H$_2$O, and **1′**-H$^+$ ⇌ **1**-H$^+$ show that a stronger thermodynamic bias towards forming benzene oxide correlates with a narrower reaction barrier width (Fig. 4). Single point energies were computed at DLPNO-CCSD(T)/def2-TZVP

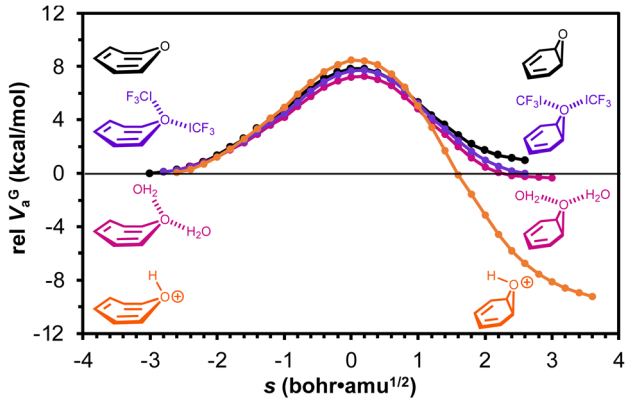

Fig. 4 Vibrationally adiabatic ground-state potential energy (V_a^G) curves for the benzene oxide → oxepin reaction (**1** → **1′**, black), and for analogous two ICF_3 coordinated (**1**-2ICF_3 → **1′**-2ICF_3, purple), two H_2O coordinated (**1**-2H_2O → **1′**-2H_2O, pink), and protonated (**1**-H^+ → **1′**-H^+, orange) reactions at DLPNO-CCSD(T)/def2-TZVP//PW6B95/def2-TZVP with frequency corrections at PW6B95/def2-TZVP. Notably, the reaction **1′**-H^+ → **1**-H^+ (orange curve) exhibits a much lower barrier width at lower energies.

with geometries and zero-point energy (ZPE) corrections at the PW6B95/def2-TZVP level.

Rate constants computed for the electrocyclizations of **1′** → **1**, **1′**-2H_2O → **1**-2H_2O, and **1′**-H^+ → **1**-H^+ without (k_{CVT}) and with the small-curvature tunnelling approximation ($k_{CVT/SCT}$) are shown in Table 2. Rate constants were computed with Polyrate[30] *via* direct dynamics based on DLPNO-CCSD(T)/def2-TZVP energies. The k_{CVT} values at a given temperature reflect the relative barrier heights for ring-opening of **1′** (8.4 kcal mol^{-1}), **1′**-2H_2O (7.7 kcal mol^{-1}), and **1′**-H^+ (8.7 kcal mol^{-1}) (*cf.* data in Fig. 3); **1′**-H^+ has the highest barrier among the three and, at any given temperature, is predicted to have the lowest rate constants without tunnelling.

Large computed $k_{CVT/SCT}$ values for **1′**-2H_2O and **1′**-H^+ document the important role of heavy-atom tunnelling in the **1′**-2H_2O → **1**-2H_2O and **1′**-H^+ → **1**-H^+ reactions (Table 2). The combination of low barrier heights (≈8–9 kcal mol^{-1}) and narrow barrier widths gives rise to large tunnelling-inclusive rate constants. For example, the $k_{CVT/SCT}$ value for **1′**-2H_2O at 10 K (2.7×10^{-4} s^{-1}, $t_{1/2}$ = 44 min) is consistent with the observation[14] that **1′**-H_2O isomerizes to **1**-H_2O under matrix isolation conditions.

The combined Arrhenius plot in Fig. 5 shows the contrast between the three systems for which we computed rate constants. For all three systems depicted, in contrast to the linear plots based on k_{CVT} values, the plots based on tunnelling-inclusive rate constants display significant curvature. The endergonic nature of **1′** → **1** means that the transformation requires some thermal energy for the reactant to climb up the barrier at least to the energy of the product before tunnelling through the barrier is possible. Thus, the Arrhenius plot based on $k_{CVT/SCT}$ values for **1′** slopes downward after it bends, which is characteristic of thermally activated tunnelling.[31] In contrast, the exergonic nature and small barrier widths for ring closure of **1′**-2H_2O and **1′**-H^+ enable deep tunnelling, *i.e.* tunnelling from the lowest vibrational state, which is characterized by temperature-independent rate constants at very low temperatures.[26]

The rate constants in Table 2 and the tunnelling-inclusive Arrhenius plots in Fig. 5 convey that the predicted $k_{CVT/SCT}$ values for **1′**-H^+ are smaller than those for **1′**-2H_2O. Based on the narrower barrier width for **1′**-H^+ relative to **1′**-2H_2O (Fig. 4), one might expect **1′**-H^+ to have a larger rate constant than **1′**-2H_2O at low temperatures. While the computed $k_{CVT/SCT}$ values are within an order of magnitude of each other, our results suggest cyclization of **1′**-2H_2O is faster than that of **1′**-H^+. The explanation for this is likely due to the 1.0 kcal mol^{-1} higher barrier for **1′**-H^+ relative to **1′**-2H_2O. It may also be connected to the effect of noncovalent interactions on the computation of necessary quantities for tunnelling transmission coefficients. Nevertheless, the pronounced effect of the narrower barrier for **1′**-H^+ (due to stronger geminal hyperconjugation in **1**-H^+) appears in the

Table 2 Computed rate constants (s^{-1}), half-lives, and tunnelling transmission coefficients for electrocyclization reactions of **1′**, **1′**-2H_2O, and **1′**-H^+

Cmpd	T (K)	k_{CVT}	$k_{CVT/SCT}$	$t_{1/2}$[a] (s)	κ[b]
1′	10	3.4×10^{-161}	4.2×10^{-25}	1.7×10^{24}	1.2×10^{136}
	20	5.1×10^{-75}	1.1×10^{-13}	6.4×10^{12}	2.1×10^{61}
	50	4.3×10^{-23}	2.0×10^{-6}	3.4×10^{5}	4.8×10^{16}
	100	1.2×10^{-5}	6.7×10^{-3}	1.0×10^{2}	5.6×10^{2}
1′-2H_2O	10	1.8×10^{-146}	2.7×10^{-4}	2.6×10^{3}	1.5×10^{142}
	20	1.0×10^{-67}	5.2×10^{-4}	1.3×10^{3}	5.3×10^{63}
	50	2.5×10^{-20}	1.9×10^{-3}	3.7×10^{2}	7.6×10^{16}
	100	2.1×10^{-4}	8.8×10^{-2}	7.9×10^{0}	4.1×10^{2}
1′-H^+	10	9.8×10^{-177}	2.9×10^{-5}	2.4×10^{4}	3.0×10^{171}
	20	8.7×10^{-83}	6.6×10^{-5}	1.0×10^{4}	7.6×10^{77}
	50	3.4×10^{-26}	2.8×10^{-4}	2.5×10^{3}	8.3×10^{21}
	100	3.5×10^{-7}	4.7×10^{-3}	1.5×10^{2}	1.4×10^{4}

[a] Half-life based on the tunnelling-inclusive rate constant. [b] $\kappa \geq 100$ corresponds to ≥99% tunnelling.

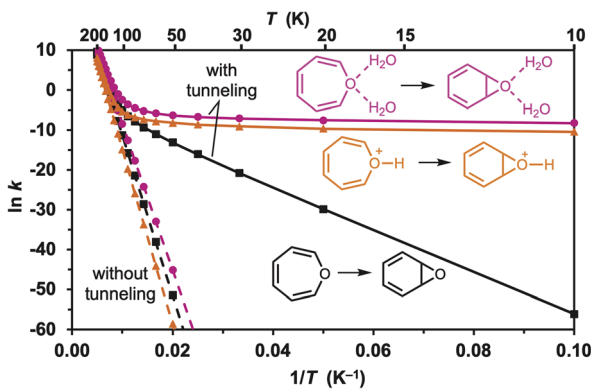

Fig. 5 Combined Arrhenius plots from computed rate constants for ring-closing of oxepin (**1′**, black), oxepin·2H_2O (**1′**-2H_2O, pink), and protonated oxepin (**1′**-H^+, orange) at the DLPNO-CCSD(T)/def2-TZVP//PW6B95/def2-TZVP level. Dashed lines indicate plots without tunnelling. Solid lines indicate plots with tunnelling included.

tunnelling transmission coefficients (kappa, κ values), which correspond to the ratio $k_{CVT/SCT}/k_{CVT}$ and reflect the rate enhancement due to tunnelling. At 10 K, κ for **1′**-H^+ is 3.0×10^{171}, which is $\approx$ 30 orders of magnitude greater than κ for **1′**-$2H_2O$ (1.5×10^{142}). Thus, our results convey the dramatic effect of protonation or Lewis acid complexation of the oxygen in **1**/**1′** on geminal hyperconjugation in these systems and the consequent feasibility of heavy-atom tunnelling at cryogenic temperatures.

Conclusions

In this work, we combined high-level electronic structure calculations and tunnelling rate computations to investigate the electronic origins of solvent- and Lewis acid-modulated rearrangements between benzene oxide (**1**) and oxepin (**1′**). Our analysis reveals that coordination of ICF_3, H_2O, or H^+ to the oxygen atom of **1** enhances geminal C–O σ → O–C σ* delocalization within the oxirane ring. This interaction strengthens and shortens the central C(1)–C(6) bond, stabilizing **1** and facilitating heavy-atom tunnelling from **1′** → **1**, in line with the directionality observed in matrix isolation experiments.[14]

These results demonstrate that geminal hyperconjugation is not merely a "mild-sort of conjugation",[22,32–34] but a powerful electronic effect for modulating quantum mechanical heavy-atom tunnelling pathways. This work extends the principle of tunnelling control[35–39] by identifying a structural and electronic feature (*i.e.*, geminal hyperconjugation) that can be tuned through weak coordination. Given the prevalence of three-membered rings in tunnelling-prone systems (*e.g.*, benzene imine, norcaradiene, semibullvalene, benzazirine), modulating geminal hyperconjugation may serve as a general strategy for controlling heavy-atom tunnelling in strained ring systems.

Computational details

All computations were performed in either Gaussian 16 (ref. 40) or ORCA[41] software suites or Polyrate 2010-A:[30] geometry optimizations and frequencies were run in Gaussian and single-point electronic energy corrections in ORCA. The absence of any imaginary normal-mode frequencies (*i.e.*, negative eigenvalues) confirmed optimized minima. The PW6B95/def2-TZVP[42,43] level of theory afforded a reasonable balance of accuracy and computational cost and has been shown in previous studies to be adequate for computing isomerizations of cycloheptatrienes and norcaradienes.[44–46] The electronic energies were corrected on the PW6B95/def2-TZVP stationary points using DLPNO-CCSD(T)/def2-TZVP.[47] Rate constant calculations were performed initially at the PW6B95/def2-TZVP level of theory, using a step size of 0.01 bohr. The interpolated single point energy (ISPE) method was then employed to modify the DFT energy surface to match the DLPNO-CCSD(T)/def2-TZVP//PW6B95/def2-TZVP energies. Tunnelling transmission coefficients were obtained using ZPE-corrected energy profiles. CVT/SCT calculations were performed following the procedure described by Truhlar *et al.*[48–50]

Author contributions

CJL: electronic structure calculations, data analysis, conceptualization. IJ: rate calculations, data analysis. TS: conceptualization, writing. WLK: rate calculations, data analysis, conceptualization, writing. JIW: conceptualization, writing.

Conflicts of interest

There are no conflicts to declare.

Data availability

Cartesian coordinates for all structures, natural bond orbital (NBO) second order perturbation energies $E(2)$, computed rate constants and sample input for rate constant calculations have been uploaded as part of the SI. See DOI: **https://doi.org/10.1039/d5sc02914g**.

Acknowledgements

J. I. W. thanks the National Institute of General Medical Sciences of the National Institutes of Health (R35GM133548) for support. W. L. K. thanks the National Science Foundation (CHE-2102160) for support, and Joscelyn Huynh for preliminary calculations. We thank the Research Computing Data Core at the University of Houston for computational resources.

Notes and references

1 N. Mandal, A. Das, C. Hajra and A. Datta, *Chem. Sci.*, 2022, **13**, 704–712.
2 J. García de la Concepción, J. C. Corchado, P. Cintas and R. Babiano, *J. Org. Chem.*, 2024, **89**, 9336–9343.
3 T. Schleif, *Chem.–Eur. J.*, 2022, **28**, e202201775.
4 J. P. L. Roque, C. M. Nunes, F. Saito, B. Bernhardt, R. Fausto and P. R. Schreiner, *ChemistryEurope*, 2025, **3**, e202400060.
5 C. M. Nunes, A. K. Eckhardt, I. Reva, R. Fausto and P. R. Schreiner, *J. Am. Chem. Soc.*, 2019, **141**, 14340–14348.
6 C. M. Nunes, I. Reva, S. Kozuch, R. J. McMahon and R. Fausto, *J. Am. Chem. Soc.*, 2017, **139**, 17649–17659.
7 J. F. Rowen, F. Beyer, T. Schleif and W. Sander, *J. Org. Chem.*, 2023, **88**, 7893–7900.
8 T. Schleif, J. Mieres-Perez, S. Henkel, E. Mendez-Vega, H. Inui, R. J. McMahon and W. Sander, *J. Org. Chem.*, 2019, **84**, 16013–16018.
9 H. Inui, K. Sawada, S. Oishi, K. Ushida and R. J. McMahon, *J. Am. Chem. Soc.*, 2013, **135**, 10246–10249.
10 C. M. Nunes, S. Doddipatla, G. F. Loureiro, J. P. L. Roque, N. A. M. Pereira, T. M. V. D. Pinho e Melo and R. Fausto, *Chem.–Eur. J.*, 2022, **28**, e202202306.
11 M. Prado Merini, T. Schleif and W. Sander, *Angew. Chem., Int. Ed.*, 2023, **62**, e202309717.
12 F. Weinhold and C. Landis, *Valency and Bonding: A Natural Bond Orbital Donor-Acceptor Perspective*, Cambridge University Press, 2005.

13 A. J. Sterling, R. C. Smith, E. A. Anderson and F. Duarte, *J. Org. Chem.*, 2024, **89**, 9979–9989.
14 T. Schleif, M. Prado Merini and W. Sander, *Angew. Chem., Int. Ed.*, 2020, **59**, 20318–20322.
15 S. Henkel, M. Prado Merini, E. Mendez-Vega and W. Sander, *Chem. Sci.*, 2021, **12**, 11013–11019.
16 E. Vogel, W. A. Böll and H. Günther, *Tetrahedron Lett.*, 1965, **6**, 609–615.
17 W.-D. Stohrer and R. Hoffmann, *Angew. Chem., Int. Ed.*, 1972, **11**, 825–826.
18 E. D. Glendening, A. E. Reed, J. E. Carpenter and F. Weinhold, *NBO Version 3.1*, Gaussian Inc., Pittsburgh, 2003.
19 F. Weinhold, C. R. Landis and E. D. Glendening, *Int. Rev. Phys. Chem.*, 2016, **35**, 399–440.
20 S. Inagaki, N. Goto and K. Yoshikawa, *J. Am. Chem. Soc.*, 1991, **113**, 7144–7146.
21 S. Inagaki, Y. Ishitani and T. Kakefu, *J. Am. Chem. Soc.*, 1994, **116**, 5954–5958.
22 J. I. Wu and P. v. R. Schleyer, *Pure Appl. Chem.*, 2013, **85**, 921–940.
23 R. E. Parker and N. S. Isaacs, *Chem. Rev.*, 1959, **59**, 737–799.
24 A. A. Zavitsas, *J. Phys. Chem. A*, 2003, **107**, 897–898.
25 W. T. Borden, *WIREs Comput. Mol. Sci.*, 2016, **6**, 20–46.
26 J. Meisner and J. Kästner, *Angew. Chem., Int. Ed.*, 2016, **55**, 5400–5413.
27 C. Castro and W. L. Karney, *Angew. Chem., Int. Ed.*, 2020, **59**, 8355–8366.
28 A. Nandi, G. Molpeceres, P. K. Gupta, D. T. Major, J. Kästner, J. M. L. Martin and S. Kozuch, *Comprehensive Computational Chemistry*, 2024, vol. 4, pp. 713–734.
29 G. Qiu and P. R. Schreiner, *ACS Cent. Sci.*, 2023, **9**, 2129–2137.
30 J. Zheng, S. Zhang, B. J. Lynch, J. C. Corchado, Y.-Y. Chuang, P. L. Fast, W.-P. Hu, Y.-P. Liu, G. C. Lynch, K. A. Nguyen, C. F. Jackels, A. F. Ramos, B. A. Ellingson, V. S. Melissas, J. Villà, I. Rossi, E. L. Coitiño, J. Pu, T. V. Albu, R. Steckler, B. C. Garrett, A. D. Isaacson and D. G. Truhlar, *POLYRATE–Version 2010A*, University of Minnesota, Minneapolis, MN, 2010.
31 E. M. Greer, K. Kwon, A. Greer and C. Doubleday, *Tetrahedron*, 2016, **72**, 7357–7373.
32 R. S. Mulliken, *Phys. Rev.*, 1933, **43**, 279.
33 R. S. Mulliken, *J. Chem. Phys.*, 1939, **7**, 339.
34 R. S. Mulliken, C. A. Rieke and W. G. Brown, *J. Am. Chem. Soc.*, 1941, **63**, 41.
35 P. R. Schreiner, *J. Am. Chem. Soc.*, 2017, **139**, 15276–15283.
36 D. Ley, D. Gerbig and P. R. Schreiner, *Org. Biomol. Chem.*, 2012, **10**, 3781–3790.
37 P. R. Schreiner, H. P. Reisenauer, D. Ley, D. Gerbig, C.-H. Wu and W. D. Allen, *Science*, 2011, **332**, 1300.
38 C. M. Nunes, J. P. L. Roque, S. Doddipatla, S. A. Wood, R. J. McMahon and R. Fausto, *J. Am. Chem. Soc.*, 2022, **144**, 20866–20874.
39 T. Schleif, M. Prado Merini, S. Henkel and W. Sander, *Acc. Chem. Res.*, 2022, **55**, 2180–2190.
40 M. J. Frisch, G. W. Trucks, H. B. Schlegel, G. E. Scuseria, M. A. Robb, J. R. Cheeseman, G. Scalmani, V. Barone, G. A. Petersson, H. Nakatsuji, X. Li, M. Caricato, A. V. Marenich, J. Bloino, B. G. Janesko, R. Gomperts, B. Mennucci, H. P. Hratchian, J. V. Ortiz, A. F. Izmaylov, J. L. Sonnenberg, D. Williams-Young, F. Ding, F. Lipparini, F. Egidi, J. Goings, B. Peng, A. Petrone, T. Henderson, D. Ranasinghe, V. G. Zakrzewski, J. Gao, N. Rega, G. Zheng, W. Liang, M. Hada, M. Ehara, K. Toyota, R. Fukuda, J. Hasegawa, M. Ishida, T. Nakajima, Y. Honda, O. Kitao, H. Nakai, T. Vreven, K. Throssel, J. A. Montgomery Jr, J. E. Peralta, F. Ogliaro, M. J. Bearpark, J. J. Heyd, E. N. Brothers, K. N. Kudin, V. N. Staroverov, T. A. Keith, R. Kobayashi, J. Normand, K. Raghavachari, A. P. Rendell, J. C. Burant, S. S. Iyengar, J. Tomasi, M. Cossi, J. M. Millam, M. Klene, C. Adamo, R. Cammi, J. W. Ochterski, R. L. Martin, K. Morokuma, O. Farkas, J. B. Foresman and D. J. Fox, *Gaussian 16, Revision C.01*, Gaussian, Inc., Wallingford, CT, 2016.
41 F. Neese, Software update: the ORCA program system – Version 5.0, *WIREs Comput. Mol. Sci.*, 2022, **12**, e1606.
42 Y. Zhao and D. G. Truhlar, *J. Phys. Chem. A*, 2005, **109**, 5656–5667.
43 A. Schäfer, H. Horn and R. J. Ahlrichs, *J. Chem. Phys.*, 1992, **97**, 2571–2577.
44 A. Karton, *Chem. Phys.*, 2021, **540**, 111013.
45 C. J. Laconsay and D. J. Tantillo, *J. Org. Chem.*, 2023, **88**, 9056–9065.
46 P.-P. Chen, J. I. Seeman and K. N. Houk, *Angew. Chem., Int. Ed.*, 2020, **59**, 12506–12519.
47 C. Riplinger, P. Pinski, U. Becker, E. F. Valeev and F. Neese, *J. Chem. Phys.*, 2016, **144**, 024109.
48 D. G. Truhlar, *Tunnelling in Molecules: Nuclear Quantum Effects from Bio to Physical Chemistry*, The Royal Society of Chemistry, 1st edn, 2020.
49 D. G. Truhlar and B. C. Garrett, *Acc. Chem. Res.*, 1980, **13**, 440–448.
50 Y. P. Liu, G. C. Lynch, T. N. Truong, D. H. Lu, D. G. Truhlar and B. C. Garrett, *J. Am. Chem. Soc.*, 1993, **115**, 2408–2415.